ELSEVIER

Thermochimica Acta 372 (2001) 75–83

thermochimica acta

www.elsevier.com/locate/tca

Heat capacities, phase transitions and structural properties of cation-exchanged H-mordenite zeolites

Mohamed Mokhtar Mohamed

Department of Chemistry, Faculty of Science, Benha University, Benha, Egypt

Received 31 August 2000; accepted 20 December 2000

Abstract

Heat capacities of hydrogen large port mordenite (H-LPM), H-LPM + Cu and Na-LPM + Cu samples have been measured in the temperature range 25–500°C before and after treatment at 400°C. The changes in weight of the samples with temperature were also examined by thermogravimetry (TG). A large change in heat capacity of a transition at 133°C appeared for the H-LPM sample before treatment. The measured heat capacity was 3.75 J g^{-1} K^{-1} that exceeds H-LPM + Cu (3.5 J g^{-1} K^{-1}) and Na-LPM + Cu (3.27 J g^{-1} K^{-1}) samples with transitions at 129 and 146°C, respectively. The transition entropies of the samples before treatment showed almost no changes. However, after treatment, the transition entropies of H-LPM, H-LPM + Cu and Na-LPM + Cu samples were 31, 15 and 0.06 kJ g^{-1} K^{-1}, respectively. These values indicated that Na^{+} and Cu^{2+} exchanged H-LPM influenced the entropy as a result of interaction of these cations with the zeolite framework. This interaction caused a diminishing of the self-diffusion of these ions. This was evidenced by the observed changes in lattice parameters of the H-LPM sample when Na^{+} and Cu^{2+} exchange took place, as measured by XRD and FT-IR spectroscopic analysis of the samples, in the range 100–1700 cm^{-1}. This confirmed that the changes in the lattice modes were related to the increase in the electrostatic interactions between the cations and the zeolite framework. The transition heat capacities of the samples after treatment were found to be in the order: Na-LPM + Cu > H-LPM + Cu > H-LPM.

Keywords: H-mordenite; Ion-exchange; Heat capacity; DSC; TG; FT-IR; XRD

1. Introduction

Zeolites are a class of porous aluminosilicates with interesting properties for industrial use [1]. Their framework generally are very open and contain channels and cavities in which cations and water molecules are located. The cation and aluminum content determine the hydrophilic or hydrophobic character of the zeolites surface since the cations compensate for the negative charge arising from the isomorphous substitution of Al^{3+} for Si^{4+} [2,3]. The content and location of water molecules depends on many factors such as the size and shape of the cavities and channels, the number and the nature of the cations in the structure and the environmental situation of the zeolite, i.e. the relative humidity and temperature [4]. It is well known that adsorbed water changes the unit cell constants, bond angles and bond lengths in molecular sieves. It is also documented that water attacks irreversibly at high temperature, the framework of zeolites such as beta, faujasite and mordenite, etc. to give extra framework Al [5].

Previous studies have shown that the cation location depends principally on the temperature but also on the

E-mail address: tm_salama@yahoo.com (M.M. Mohamed).

0040-6031/01/$ – see front matter
PII: S0040-6031(01)00433-6

presence of adsorbed molecules [6,7]. A study on the influence of temperature on the cation distribution in calcium mordenite showed that the calcium located in small channel has the best co-ordination and its occupancy increases as the temperature rises. Whereas, the calcium ion, in large channel, suffers distributions over two pairs of sites, in both of which it is bonded to framework oxygens of the wall of the large channel and also to water molecules [8]. The influence of temperature on the cation distribution inside zeolites is opposite to what would be expected for Boltzmann distribution who mentioned the even distribution of the cation as the temperature increases [9].

A computational approach was carried out for locating Ni^{2+} ions in siliceous mordenite zeolite [10]. It has been found that Ni^{2+} ions are indeed related to the distribution and sitting of aluminum present in the Al–O–(Si–O)$_n$–Al sequences in the siliceous lattice. The cation–framework interaction discussed by Kaliaguine and co-workers [11] through an XPS study showed that the larger the electropositivity of the counter cation the lower are the binding energies of the framework element (Si 2p, Al 2p and O 1s). However, the extent of these changes depends strongly on the Si/Al ratio of zeolites.

The location and behavior of cations inside zeolites with temperature are still a matter of debates especially if the zeolite water content is considered. These debates come from the minute changes perceived in the lattice and channel dimensions although of the wide variations in cation occupancies [12]. More information on the cation-exchanged zeolites can be achieved through applying the heat capacity measurements on the H-LPM, H-LPM + Cu and Na-LPM + Cu samples. Special interest was given to studying the samples at phase transitions to reveal the host–guest interaction within hydrated and dehydrated cation-exchanged mordenite zeolite. These transitions were studied from both thermodynamic and structural point of views.

2. Experimental

2.1. Materials

The H-form of mordenite (H-LPM; hydrogen large port mordenite) was prepared from the Na-mordenite by exchanging 20 g during 24 h with 1 l 1N NH_4Cl solution at room temperature. This treatment was repeated twice and the final NH_4-LPM was filtered off, washed until Cl free and dried at 50°C in air. The H-LPM was obtained by calcining the ammoniated form stepwise (0.5°C min^{-1}) up to 500°C to avoid changes of the zeolite lattice. The copper exchanged mordenite samples (Na-LPM + Cu and H-LPM + Cu) were prepared by refluxing the Na-form as well as H-form with solution of $Cu(NO_3)_2$, the concentration of which were determined by assuming an exchange efficiency level of 80%. To ensure stoichiometric exchange, the pH of the nitrate solution was kept at ca. 6. The samples were dried at 100°C for 24 h and then calcined at 500°C at a rate of 0.5°C min^{-1}.

2.2. Techniques

Infrared spectra were recorded on a Perkin-Elmer FT-IR 1650 spectrometer at room temperature after heating the samples at 400°C for 2 h. Mid-infrared and far-infrared (1700–100 cm^{-1}) spectra were recorded using a self-supporting sample (3–8 mg cm^{-1}), 200 scans were averaged at a resolution of 2 cm^{-1} using DTGS detector.

X-ray diffraction patterns were taken in order to characterize the samples phases, crystallinities and unit cell parameters. The patterns were obtained with the help of the Philips PW 213/00 apparatus. The measurements were run with nickel-filtered Cu Kα ($\lambda = 1.5405$ Å) at 35 kV and 20 mA at a scanning rate of $2\theta = 2^\circ$ min^{-1}.

The specific heat, C_p, was determined for the samples using a differential scanning calorimeter (DSC) technique where a Shimadzu DSC TA 50 thermal analyzer was used. Before carrying out the heat capacity measurements, the samples were heated under N_2 atmosphere at 400°C for comparison with those before heating.

The measurements were made by applying the relationship as follows:

$$C_s - C_r = \frac{T_s^{st} - T_r^{st}}{\alpha R}$$

where C_s and C_r are the heat capacities of both the sample and the reference sides, respectively, α the rate of temperature rise, T_s^{st} the rate of temperature of

sample side in stable state, T_r^{st} the temperature of reference side in stable state, R the instrument constant (resistance between sample/reference sides and furnace).

Accordingly, $T_s^{st} - T_r^{st}$ represents DSC output, which is proportional to the difference in heat capacities of the samples and reference sides. Therefore, if DSC output is S and proportion constant is k, the following may be expressed as

$$C_s - C_r = kS$$

Under these conditions, the DSC will appear as a measured curve. Actual measurement for the specific heat analysis was measured when the following three configuration were carried out.

1. One measurement with nothing in the sample crucible (blank).
2. Measurement of a reference material (known specific heat capacities, e.g. alumina) weighing m_0 (g) in sample crucible.
3. Measurement of a sample of unknown specific heat capacity weighing m (g) in sample crucible. When measurement is performed, an empty sample crucible is always placed on the reference side. The respective heat capacities of sample and reference are designated as C_s^h and C_r^h, and reference material and sample specific heat capacities are C_0 and C, respectively. The following three equations are used to represent the measurement in each of the above configuration.

$$C_s^h - C_r^h = kS_1 \quad (1)$$

$$(C_s^h + m_0c_0) - C_r^h = kS_2 \quad (2)$$

$$(C_c^h + mc) - C_r^h = kS_3 \quad (3)$$

where S_1, S_2 and S_3 are the DSC signals during measurement in stable state. From $3 - 1/2 - 1$, $mc/m_0c_0 = (S_3 - S_1)/(S_2 - S_1)$.

Accordingly, the specific heat capacities of the sample can be considered to be

$$C = \frac{m_0c_0}{m}\frac{S_3 - S_1}{S_2 - S_1} \quad (4)$$

The specific heat capacity of the sample can be determined on the basis of Eq. (4). The samples were subjected to thermogravimetric (TG) analysis over the temperature range from ambient to 600°C (2°C min^{-1}) under a N_2 atmosphere (30 cm^3 min^{-1}). TG curves were automatically recorded on a Shimadzu TG 50 unit.

3. Results and discussion

The heat capacities of H-LPM, H-LPM + Cu and Na-LPM + Cu samples are plotted in Figs. 1–3, respectively. These samples were measured before and after heating at 400°C in a flow of N_2. Besides, an integral TG curve was included in each figure for examining the thermodesorption behavior of the samples.

A phase transition at 133°C for the H-LPM sample was observed before heating (Fig. 1) however, after heating, a phase transition at 235°C was obtained. An anomaly increase in the heat capacity around 307 and 327°C was depicted for both heated and non-heated samples, respectively. It can be seen that the heat capacity values of the non-heated H-LPM sample were higher than those for heated in almost all the temperature range except behind the anomaly the increase in the specific heat for the heated sample was higher. The TG curve for the sample illustrates a sharp desorption for the sample before heating whereas a minute weight loss is indicated after heating. This indicates the dependence of the heat capacity on the water content for the non-heated sample (hydrated); putting into consideration the stability of the sample throughout all the temperature range to conclude that the loss corresponds only to the zeolite water content. Thus, the heat capacity of the sample before heating approaches that of water. However, the protons, associated with negatively charged framework oxygens, and their mobilities become the governing parameters affect the heat capacities after dehydration. Therefore, one can attribute the rapid increase in the heat capacity at transition for both dehydrated and hydrated sample to the protonic movement provoked by water leaving adsorption sites within the channel system.

Fig. 2 shows the heat capacity change and loss in weight for the H-LPM + Cu sample with temperature. This sample showed the same trend as that seen for the H-LPM sample. However, the estimated heat capacity values for the H-LPM + Cu sample were lower than

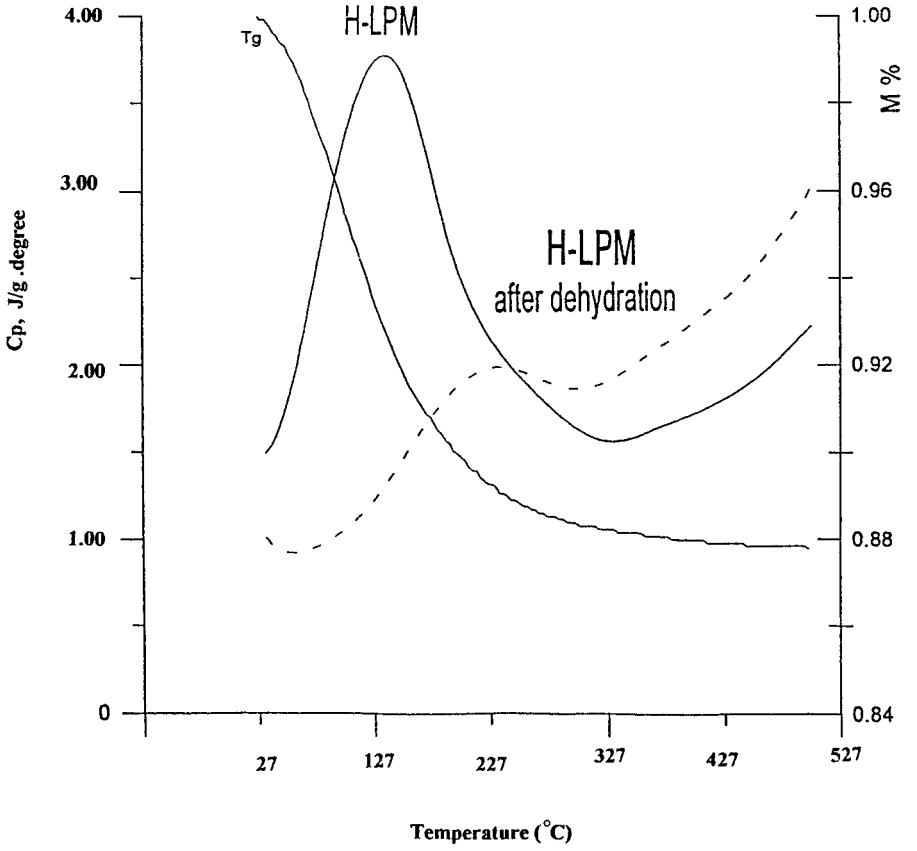

Fig. 1. The variation of specific heat (C_p) and weight loss (TG) with temperature for the H-LPM sample before and after dehydration at 400°C.

those of the H-LPM one, although of comparable transition temperatures before dehydration. This is attributed to the replacement of some hydroxyl groups of H-LPM with Cu cations that results in a decrease in the ionic character, i.e. a covalent bond between oxygen and Cu is expected to increase.

Fig. 3 shows the heat capacity change and loss in weight for the Na-LPM + Cu sample with temperature. A broad phase transition with a maximum at 146°C indicated, before dehydration, a heat capacity value of 3.27 J g^{-1} K^{-1}. Besides, a small hump at 327°C was noticed at the tail of the peak, beyond it a small increase in the heat capacity took place. An asymmetric peak after dehydration of a transition at 267°C was observed that showed a heat capacity value of 2.97 J g^{-1} K^{-1}. The prominent appearance of the broad shape at the phase transition before and after dehydration indicates the existence of some residual bound water that strongly co-ordinated to Na^+ ions. This result is ascertained by noting the integral TG curve that showed the mass loss continuation even after heating at 400°C. For the Na^+ free sample, a less water in total is observed (Fig. 2) due to the larger size of Cu^{2+} ions. The same result is concluded in Table 1. The hump at 327°C was not observed in Figs. 1 and 2. This hump could be originated from site heterogeneity of the Na^+ ions within the mordenite framework. It could also be correlated to the existence of highly energetic phase provoked by Na^+ cations. A similar peak in a DSC study for the Na-LPM sample was confirmed by Mohamed [12] who attributed it to the interaction of Na^+ ions with H_2O molecules.

More informations concerning the appearing of this hump are obtained from the XRD pattern of the

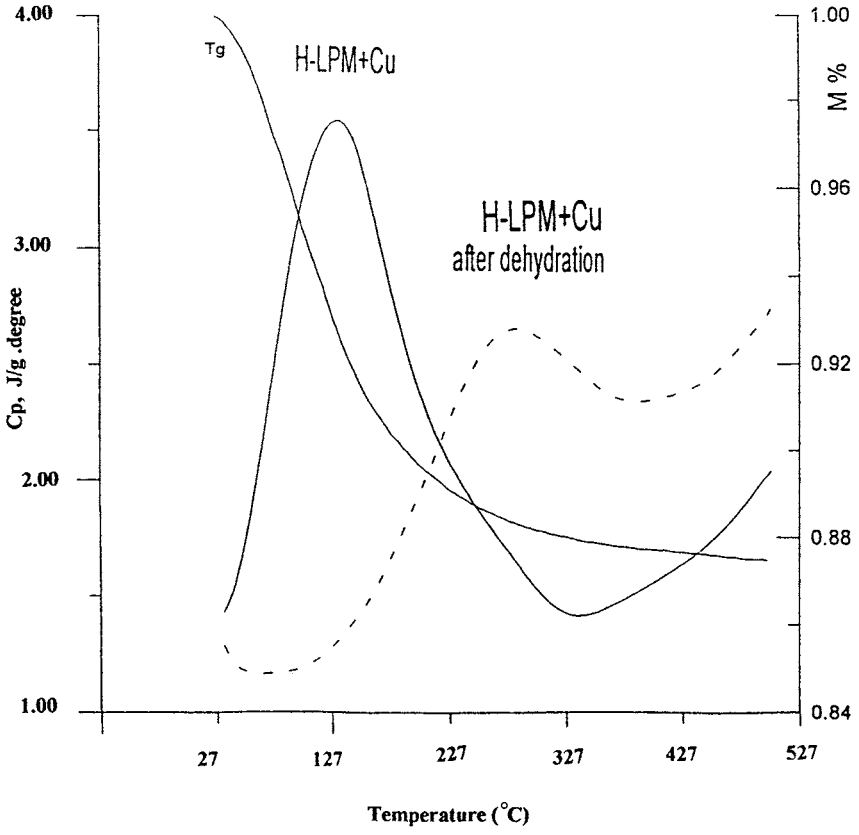

Fig. 2. The variation of specific heat (C_p) and weight loss (TG) with temperature for the H-LPM + Cu sample before and after dehydration at 400°C.

sample that showed new peaks at $d = 6.41, 4.91, 4.16$ and 1.87 Å those represented by arrows in the XRD pattern (Fig. 4), which cannot be identified. These peaks were not seen in the pattern of the H-LPM + Cu sample. Thus, the presence of new peaks in the Na-LPM + Cu sample may be explained by the partially cationic-exchange between sodium and copper phases, which took place in the framework, leading to the formation of cationic vacancies and new phase with defective structure, i.e. a displacive phase transition without change in symmetry. Furthermore, the marked contraction in the lattice parameter b_0 for the Na-LPM + Cu sample and the significant decrease in crystallinity compared with the others, as depicted in Table 1, indicate that Na^+ interacted to form a new phase.

It is worthy noting that the heat capacity, C_p, values decrease in the order H-LPM > H-LPM + Cu > Na-LPM + Cu before dehydration. Insertion of Cu into H-LPM causes a small decrease in the heat capacity $(C_p)_{max}$ value. However, a remarkable depression by lowering the transition point $(C_p)_{max}$, was indicated upon introducing Na^+ and Cu^{2+} cations, as depicted in the Na-LPM + Cu sample. This effect can be explained by structural changes at the aluminum site induced by increased repulsion (both steric and electrostatic) between cations in the case of Na-LPM + Cu and decreased repulsion in the case of H-LPM + Cu. This explanation is further confirmed by the perceived changes in the ionic radius of the cations: Cu^{2+}, 0.72 Å and Na^+, 0.97 Å. One Cu^{2+} cation induces less structural changes than two Na^+ cations in the same volume during substitution.

On the other hand, after dehydration, the nature of interaction forces of inserted ions with the framework oxygen is quite important because of considerable

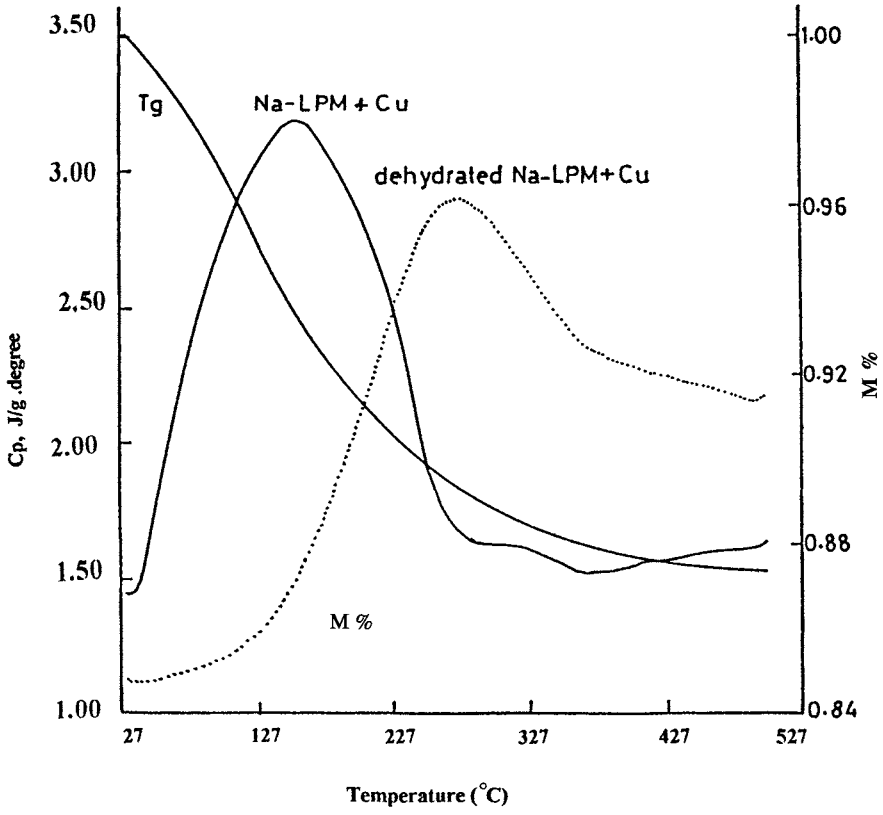

Fig. 3. The variation of specific heat (C_p) and weight loss (TG) with temperature for the Na-LPM + Cu sample before and after dehydration at 400°C.

diminution of the cations diffusion, as has been investigated for the NaCaA zeolite sample [13,14]. This resulted from the strong interaction between the cations and the zeolite lattice. This is envisaged from significant changes in lattice parameters, as detected from X-ray experiments (Table 1), as well as the major variation in the framework vibrations, as examined by IR spectroscopy (Fig. 5). A strong interaction between

Table 1
Unit cell dimensions, crystallinities and water content of the studied samples

Sample	Unit cell dimensions (Å)			Volume (Å)[3a]	Crystallinity[b]	Ratio of the intensities, A/B[c]	Water content (wt.%)
	a_0	b_0	c_0				
H-LPM	18.248	20.494	7.497	2803.69	100	0.67	8.07
H-LPM + Cu	18.329	20.525	7.509	2824.91	95.9	0.62	8.15
Na-LPM + Cu	18.377	20.511	7.547	2844.70	81.4	0.50	14.5

[a] Volume denotes the unit cell volume $a \times b \times c$.

[b] The crystallinity was obtained from the sum of the intensities of the (1 1 1), (2 4 1), (0 0 2), (2 0 0), (5 1 1), (1 5 0) and (3 5 0) diffraction lines. The H-mordenite is taken as reference 100% crystallinity.

[c] The ratio of the intensities of 578–566 cm^{-1} (A) and 472–455 cm^{-1} (B) bands is a quantitative measure of the crystallinity of zeolite. For a well-crystallized H-mordenite sample, the absorbance ratio (A/B) is close to 0.7.

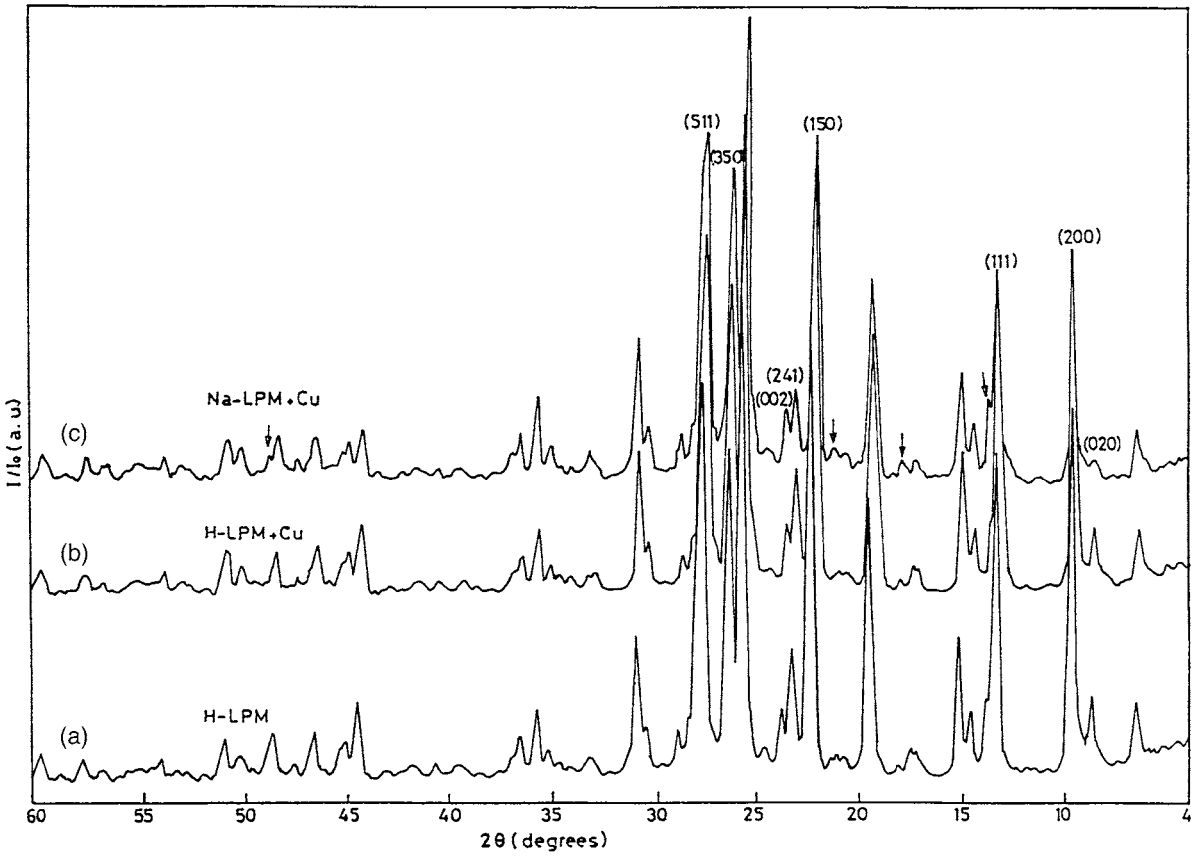

Fig. 4. XRD patterns of (a) H-LPM; (b) H-LPM + Cu; (c) Na-LPM + Cu samples heated at 400°C.

Na^+ ions and the lattice is depicted, through the appreciable diminishing of the bands at 199 and 257 cm^{-1} that was higher than that with copper ones. This was due to the highly weighted cations in the Na-LPM + Cu sample compared with the H-LPM + Cu one that induces less vibrational changes. The disappearance of the shoulder at 322 cm^{-1} that can be correlated to Cu^{2+} cations after Na^+ incorporation is further emphasized by the localization of both mono- and divalent-ions in same sites. The 114 cm^{-1} band observed in the Na-LPM + Cu sample, which was not detected in the H-LPM + Cu one, is attributed to vibrations of Na^+ cation relative to the framework. This assignment was in agreement with that detected for Na-Y zeolite after heating [15]. The 114 cm^{-1} band disappears completely after treatment with HCl solution to further confirm that assigning this band to the Na^+ vibrations in mordenite is accurate. The existence of solely a single band at 114 cm^{-1} for the Na-LPM + Cu sample indicates the absence of Na^+ cations with different energy states in mordenite.

The thermodynamic quantities (temperature, enthalpy and entropy) related to the transition before and after dehydration are summarized in Table 2. Evidently, the entropy at the transition ΔS calculated by $\Delta H/T_{max}$ for H-LPM and H-LPM + Cu samples showed no changes before dehydration. However, a small effect was only detected for the Na-LPM + Cu sample. This explains the high ordering of the samples before dehydration, i.e. the stability of the phase transition is governed by its energy rather than its entropy in the low temperature range. On the other hand, after dehydration, a high disordering process, described by high and varied ΔS values, was revealed

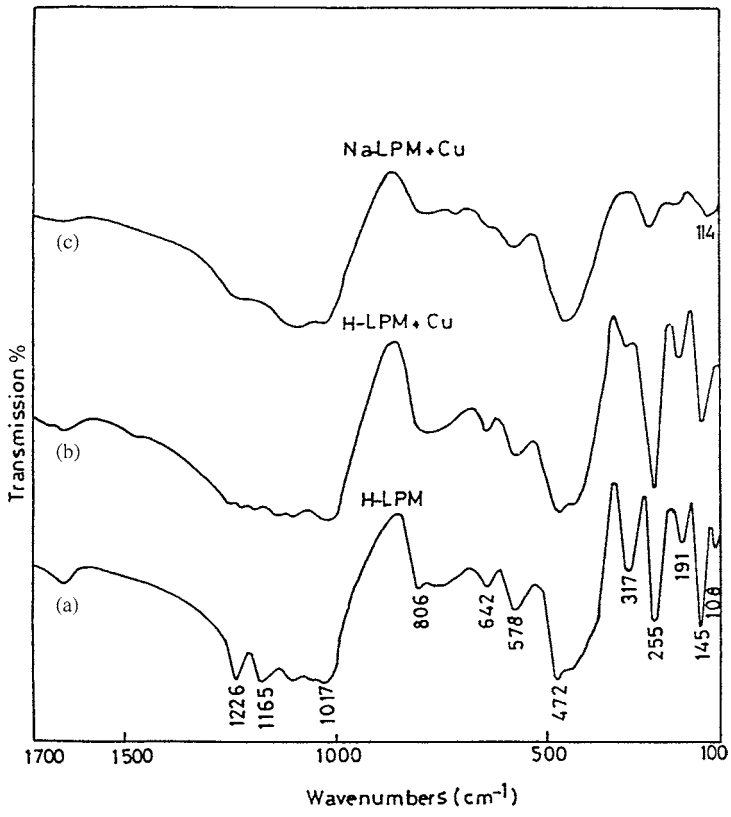

Fig. 5. FT-IR spectra in the 1700–100 cm^{-1} range of (a) H-LPM; (b) H-LPM + Cu; (c) Na-LPM + Cu samples heated at 400°C.

for the samples to be in the order: H-LPM > H-LPM + Cu > Na-LPM + Cu, i.e. Na^+ and Cu^{2+} ions induce long-range interactions depressing the disordering properties of the acidic H-protons in the H-LPM sample. Na^+ ions effectively suppress the mobility of the H-protons in the H-LPM sample when Na^+ substitution took place. The encountered varied samples order between heat capacities (Na-LPM +Cu > H-LPM + Cu > H-LPM) and entropies (H-LPM > H-LPM+Cu > Na-LPM + Cu), after dehydration, requires the participation of not only thermodynamic but also structural point of views, as has been presented. It is likely that ΔS value measures the mobility of the protons attached to bridging OH groups (acidic protons) that are more influenced to temperature than the silanol ones. Thus, ΔS indicates high value for the H-LPM sample compared with the other samples. Whereas, the specific heat, C_p, is governed by structural changes (electrostatic, ionic radius, mass, volume and nature of interaction) after dehydration. Most probably, the mass effect on the vibrational modes of the Na-LPM + Cu sample was responsible for enhancing the heat capacity values compared to the others [16].

Table 2
Temperature, enthalpies and entropies of the phase transitions of H-LPM, H-LPM + Cu and Na-LPM + Cu samples before and after heating at 400°C

Sample	$T_{transition}$ (°C)	ΔH (k J g^{-1})	ΔS (kJ g^{-1} K^{-1} × 100)
H-LPM			
Before	133	0.52	0.39
After	235	73.39	31
H-LPM + Cu			
Before	129	0.52	0.4
After	282	41.01	15
Na-LPM + Cu			
Before	146	0.39	0.3
After	267	0.15	0.06

4. Conclusions

The heat capacity study indicates variations in the H-mordenite framework–cation interaction before and after dehydration for the H-LPM, H-LPM + Cu and Na-LPM + Cu samples. These variations were measured between 25 and 500°C with special attention paid to the phase transitions occurred in the temperature ranges 129–136°C and 235–282°C for both hydrated and dehydrated samples, respectively.

The heat capacity for the H-LPM sample exhibited high values compared with H-LPM + Cu and Na-LPM + Cu samples before dehydration. Insertion of Na^+ cations beside Cu ones altered the phase transition for the Na-LPM + Cu sample, compared with the H-LPM one, to be accompanied by: (a) considerable decrease in $(C_p)_{max}$; (b) broadening in the phase transition peak; (c) a small hump at 327°C; (d) a significant decrease in entropy at the transition. The entropy change of the samples before dehydration showed almost no alteration, i.e. stable phase transitions of the samples due to their lower free energy. Thus, the margin of change of phase transitions was small before dehydration for the samples (129–136°C).

On the other hand, after dehydration, a reversed phenomenon for the heat capacity order was observed to be: Na-LPM + Cu > H-LPM + Cu > H-LPM. This behavior cannot be correlated with the thermodynamic parameters that showed the highest ΔS value for the H-LPM sample. Therefore, structural studies were the governing factors influencing the behavior of the phase transition. This was apparent as: (a) from IR results, it was evident that dehydration not only affect the cation modes observed in the FIR region but also the lattice modes were significantly affected; (b) the nature of these changes was strongly enhanced in the Na-LPM + Cu sample that showed the lowest crystallinity; (c) in the Na-LPM + Cu sample, significant changes in unit cell constants were well assured compared with the other samples.

References

[1] H. van Bekkum, E.M. Flanigen, J.C. Jansen (Eds.), Introduction to Zeolite Science and Practice, Studies in Surface Science and Catalysis, Vol. 58, Elsevier, Amsterdam, 1991.
[2] D.W. Breck, Zeolite Molecular Sieves, Wiley, New York, 1974.
[3] J.V. Smith, Chem. Rev. 88 (1988) 149.
[4] A. Dyer, An Introduction to Zeolite Molecular Sieves, Wiley, New York, 1988.
[5] D. Barthomeuf, Stud. Surf. Sci. Catal. 105 (1996) 1677.
[6] W.J. Mortier, J. Phys. Chem. 81 (1977) 1334.
[7] W.J. Mortier, J.J. Pluth, J.V. Smith, Mater. Res. Bull. 10 (1975) 1037.
[8] J. Elsen, G.S.D. King, W.J. Mortier, J. Phys. Chem. 91 (1987) 5800.
[9] W.J. Mortier, J. Phys. Chem. 79 (1975) 1447.
[10] C.J.J. Den Ouden, R.A. Jackson, C.R.A. Catlow, M.F.M. Port, J. Phys. Chem. 94 (1990) 5286.
[11] M. Huang, A. Adont, S. Kaliaguine, J. Am. Chem. Soc. 114 (1992) 10005.
[12] M.M. Mohamed, Thermochem. Acta 230 (1993) 167.
[13] J. Karger, D.M. Ruthven, Diffusion in Zeolites and Other Microporous Solids, Wiley, New York, 1992.
[14] R. Haberlandt, S. Fritzsche, G. Peinel, K. Heinzinger, Molekulardynamik Grundlagen und Anwendungen, Vieweg, Wiesbaden, 1995.
[15] J. Howard, J.M. Nicol, Zeolites 8 (1988) 142.
[16] N. Yamamuro-Ondo, O. Yamamuro, T. Matsuo, H. Suga, J. Phys. Chem. 100 (1996) 19647.